Final Report: September 30, 2015

DISPERSED METAL CLUSTER CATALYTS BY DESIGN: SYNTHESIS, CHARACTERIZATION, STRUCTURE, AND PERFORMANCE

Abstract: The PI's in this project (entitled **DISPERSED METAL CLUSTER CATALYTS BY DESIGN: SYNTHESIS, CHARACTERIZATION, STRUCTURE, AND PERFORMANCE**, DE-SC0005822) are Ilke Arslan, PNNL (ilke.arslan@pnnl.gov); David Dixon, Univ. Alabama (dadixon@as/ua.edu); Bruce Gates, UC Davis (bcgates@ucdavis.edu); and Alexander Katz, UC Berkeley (askatz@uclink.berkeley.edu). The graduate students were Mingyang Chen, Shengjie Zhang, and Jason Dyer (Univ. of Alabama), Ceren Aydin, Joseph Kistler, Jing Lu (in part), Louise Debefve, and, formerly, Jacob Wolf, Univ. of California Davis, and a postdoc was Andrew Solovyov, Univ. of California Berkeley. The collaborators were N. D. Browning, UCDavis/PNNL, R. Finke, Colorado State Univ., C. Y. Chen, Chevron, A. J. Liang, Chevron, S. L. Scott, University of California Santa Barbara, S. I. Zones, Chevron. Jacob Wolf left the project with no results.

To understand the class of metal cluster catalysts better and to lay a foundation for the prediction of properties leading to improved catalysts, we have synthesized metal catalysts with well-defined structures and varied the cluster structures and compositions systematically—including the ligands bonded to the metals. These ligands include supports and bulky organics that are being tuned to control both the electron transfer to or from the metal and the accessibility of reactants to influence catalytic properties. We have developed novel syntheses to prepare these well-defined catalysts with atomic-scale control the environment by choice and placement of ligands and applied state-of-the art spectroscopic, microscopic, and computational methods to determine their structures, reactivities, and catalytic properties. The ligands range from nearly flat MgO surfaces to enveloping zeolites to bulky calixarenes to provide controlled coverages of the metal clusters, while also enforcing unprecedented degrees of coordinative unsaturation at the metal site—thereby facilitating bonding and catalysis events at exposed metal atoms. With this wide range of ligand properties and our arsenal of characterization tools, we worked to achieve a deep, fundamental understanding of how to synthesize robust supported and ligand-modified metal clusters with controlled catalytic properties, thereby bridging the gap between active site structure and function in unsupported and supported metal catalysts. We used methods of organometallic and inorganic chemistry combined with surface chemistry for the precise synthesis of metal clusters and nanoparticles, characterizing them at various stages of preparation and under various conditions (including catalytic reaction conditions) and determining their structures and reactivities and how their catalytic properties depend on their compositions and structures. Key characterization methods included IR, NMR, and EXAFS spectroscopies to identify ligands on the metals and their reactions; EXAFS spectroscopy and high-resolution STEM to determine cluster framework structures and changes resulting from reactant treatment and locations of metal atoms on support surfaces; X-ray diffraction crystallography to determine full structures of cluster-ligand combinations in the absence of a support, and TEM with tomographic methods to observe individual metal atoms and determine three-dimensional structures of catalysts. Electronic structure calculations were used to verify and interpret spectra and extend the understanding of reactivity beyond what is measurable experimentally.

Key results in bullet form:

- When synthesizing coordinatively unsaturated (decarbonylated) clusters of the family $Ir_4(CO)_X(phosphine)_{12-X}$, we observed a preferential ability to stabilize the cluster in a decarbonylated state when using large ligands such as calixarene phosphines relative to the isoelectronic but slightly smaller $MeP(Ph)_2$. Thus a focus of our ongoing efforts is to understand

how large ligands can be exploited catalytically while enforcing stable coordinatively unsaturated sites in metal clusters.

- We used computational chemistry to predict the reaction chemistry of a family of iridium clusters of the family $Ir_n(CO)_m$ and iridium carbonyl phosphine clusters, including exothermicity of the nucleation reactions when CCSD(T) calculations are infeasible. These results link experiments such as those mentioned above with calculated results.
- We observed the first stages of metal cluster formation, using aberration-corrected STEM to image individual Ir atoms in the straight, nonintersecting pores of the zeolite SSZ-53.
- We found that sintering of iridium clusters on supports stops at a critical diameter of approximately 1 nm, with clusters of this size bouncing off each other—this "smart" catalyst in intrinsically sinter resistant.
- We reported extensive calculations characterizing complexes and small clusters of Co, Rh, and Ir on supports, finding good agreement with experimental spectra.
- We recorded the first tomographic images of a delaminated zeolite, determining its three-dimensional structure and porosity in unprecedented detail and gaining insight into the process of delamination.
- We used STEM to determine three-dimensional structures of small osmium clusters on MgO.
- We reported a segregated supported bimetallic catalyst and the influence of remote interactions of the separate metals on catalyst performance.
- We wrote a review of STEM in characterization of supported metal cluster catalysts.
- We elucidated how the ligands on mononuclear rhodium complexes and the support control aggregation of the metal to form clusters.
- We reported a new class of single-site catalyst, consisting of an apical Ir atom in a tetrahedral iridium cluster on a support, with the reactivity controlled by the ligands on the basal iridium atoms.
- We reported site isolated platinum catalysts in a zeolite and their characterization by STEM.
- We wrote a review of molecular metal catalysts on supports.
- We wrote an essay entitled "Beyond Relationships between Homogeneous and Heterogeneous Catalysis," integrating many of the viewpoints of this project.
- We reported new iridium dinitrogen complexes on zeolite HY and characterized them by density functional theory calculations.
- We demonstrated the agglomerative sintering of iridium initially atomically dispersed in zeolite HY, characterizing the first stages of cluster formation and modeling the process of sintering.
- We developed new methodology for interpretation of STEM data.
- We extended STEM measurements to a cracking catalyst containing La cations.

This research is addressing priority research needs identified by DOE, specifically in response to the challenge stated recently in a 2007 BESAC report entitled *Directing Matter and Energy: Five Challenges for Science and the Imagination*: "Major challenges in heterogeneous catalysis are to more clearly define the nature of the active sites, to engineer at the molecular level catalysis with designed properties in three dimensions, and to create new catalysts for new transformations. Major advances here will require active interplay among instrumentation specialists, synthetic chemists, and electronic structure theorists."

Introduction

Our samples were synthesized from reactive organometallic precursors chosen to allow precise control of the synthesis chemistry. The clusters on supports are chosen to be highly uniform and small (only a few metal atoms each), because the metal–ligand and metal–support interactions and the opportunities for exact structure determination are maximized. We are making progress toward examining structures,

reactivities, and catalytic behavior of some samples as the cluster frames are assembled atom by atom. Key ideas underlying the proposal are (a) the capability to precisely modify (and properly characterize) the reactive sites, (b) a selection of test reactions to characterize catalyst performance, and (c) the application of techniques that allow fundamental understanding of how the catalysts function and enable predicting the behavior of new types of catalysts. We also investigated catalysts that incorporate bulky ligands that may envelope the clusters, including large calixarene ligands that are expected to mimic supports to control access to the cluster surface as well as the electronic state of the metal.

Controlling the ligation of tetrairidium clusters

Control of open active sites for catalysis continues to be a theme that is at the state-of-the-art in catalyst synthesis. Recent observations of blockage of open sites on metals provides new routes for controlling coking, hydrogenolysis, oxidative dehydrogenation, and several other reactions; however, a heretofore unrealized goal is the control of microenvironment surrounding a coordinatively unsaturated site, beyond just site blockage, so as to dictate catalytic activity and selectivity at open sites on metal surfaces. On route to this ultimate goal, we have undertaken a broad study of synthesis of stable open metal clusters that leverages on the known stability of the Ir_4 cluster framework and research by the Gates group in this area, by choosing to investigate the system consisting of the $Ir_4(CO)_X(phosphine)_{12-X}$ family of clusters. We recently investigated the thermal decarbonylation of the clusters shown in Figures 1 and 2 (top panel) via FTIR spectroscopy with the clusters in toluene solution.

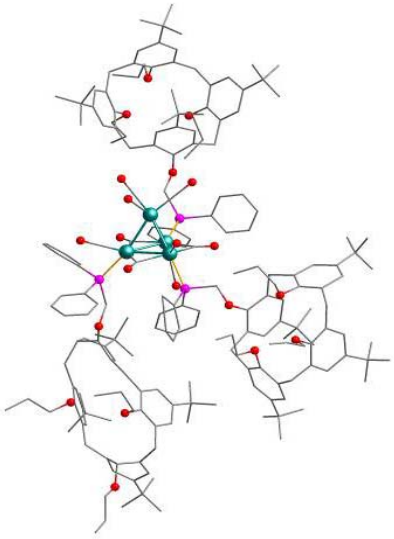

Figure 1. *X-ray structure of cluster in which X = 3 in family of clusters described by formula $Ir_4(CO)_X(phosphine)_{12-X}$, comprising calixarene phosphine ligands.*

When synthesizing open (decarbonylated) clusters of the family $Ir_4(CO)_X(phosphine)_{12-X}$, we observed a preferential ability to stabilize the cluster in a decarbonylated state when using large ligands such as calixarene phosphines, shown above, relative to isoelectronic but slightly smaller $MeP(Ph)_2$ as a ligand. Thus a focus of ongoing collaborative efforts has been to more fully understand the ability of large ligands for stabilizing open sites in metal clusters. This work has been performed by decarbonylating the clusters either thermally or by using trimethylamine oxide as a selective decarbonylation reagent, followed by a recarbonylation treatment. In a comparison of the cluster shown in Figure 1 with a homologous one in which the bulky calixarene phosphine ligand is replaced with PPh_2CH_3, dynamic light scattering data show that, upon opening of the cluster via selective decarbonylation, the calixarene-based cluster is stable, whereas the one based on the smaller PPh_2CH_3 ligand is unstable. Collaborative experiments between the Katz and Gates groups demonstrate a several-fold increase in catalytic reaction rate for the open cluster when compared with the closed cluster, even for the most simple (and structure insensitive) probe reaction consisting of ethylene hydrogenation. Current efforts are aimed at better understanding of why, and a focus on measuring H-D exchange reaction rates in the conversion of $H_2 + D_2$ with open and closed supported iridium clusters. These studies set up the possibility of varying the ligand, leveraging on our recent progress in synthesis of NHC-carbene-bound iridium clusters (reported previously). The required calixarene-bound clusters for this investigation are currently being synthesized.

The Katz and Gates group are collaborating with Arslan in the characterization of metal clusters on supports via TEM, and this has already resulted in a publication. An example image is shown in Figure 2.

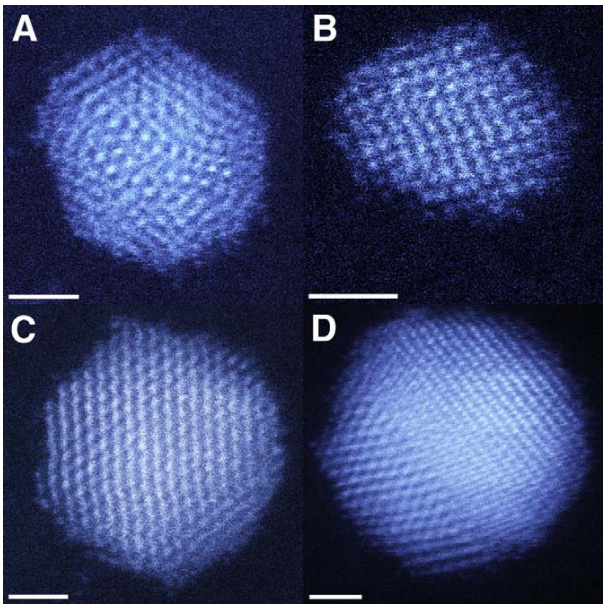

Figure 2. *(A) through (D) representative aberration-corrected micrographs of Au nanoparticles on TMS-capped SiO_2. The scale bar in each panel represents 1 nm. These images were used to quantify at atomic resolution number density of open active sites on a supported gold cluster catalyst (image represents collaboration of Katz and Arslan groups).*

Computational investigation of iridium clusters

Iridium cluster carbonyls ($Ir_n(CO)_m$) have been broadly investigated because of their rich chemistry, relatively simple metal framework structures, and their potential role in modeling of catalytic processes. The most widely investigated structure is $Ir_4(CO)_{12}$, and its derivatives have been used as soluble and supported catalysts for hydrocarbon activation and other processes. The properties of these clusters are highly relevant to the site-isolate clusters under investigation in the current project. The low-energy isomers of the $Ir_n(CO)_m$ complexes (n = 1-4, 6) were investigated by using density functional theory and coupled cluster theory. The use of the local SVWN5 functional predicted geometry parameters of high quality for $Ir_n(CO)_m$, with calculated bond lengths within 0.01 Å of experiment. $Ir_4(CO)_{12}$ is calculated to be the most favored cluster for $Ir_n(CO)_m$ reacting with CO at low temperature, and $Ir_6(CO)_{16}$ can be formed at temperatures above room temperature. Smaller $Ir_n(CO)_m$ clusters will nucleate to form $Ir_4(CO)_{12}$ spontaneously. Most of the DFT functionals, especially pure functionals, could not predict consistent reaction energies as compared to CCSD(T). The average value of the reaction energies at the MP2 and ωB97XD levels qualitatively match the CCSD(T) energies. We average the MP2 and ωB97XD reaction energies as they provide upper and lower estimates of the CCSD(T) values to predict the reaction exothermicity for the $Ir_n(CO)_m$ nucleation reactions where CCSD(T) calculations are infeasible. A summary of the reactions is shown in Figure 3. We continued to investigate various iridium clusters with various substituents, mostly phosphines, to see how the cluster structures change to model experiments such as those described above.

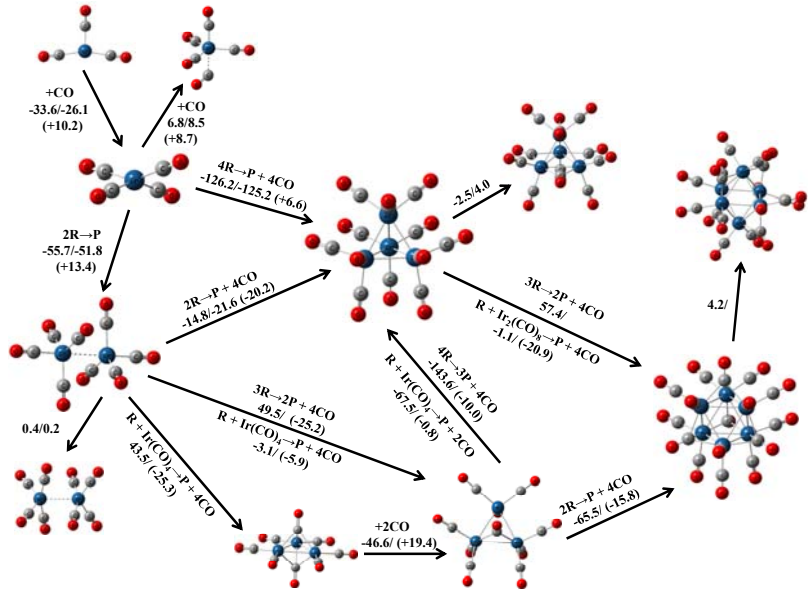

Figure 3. *Reaction energies for carbonylation of iridium clusters in kcal/mol. The first value is the average of the DFT and MP2 values with the value after the / from CCSD(T). The value in () is the ΔG correction at 298 K.*

We investigated bare iridium clusters $(Ir)_n$ up to n = 8 with high-level molecular orbital theory and density functional theory. Our results show that these structures have spatial and symmetry values different from those previously reported. Low-lying structures of the small iridium clusters Ir_n (n = 2-8) were optimized by using DFT with various functionals. Ir_2 and Ir_3 were also optimized using CASSCF methods. CCSD(T) (for Ir_2 and Ir_3), CASPT2 and MRCI (for Ir_2) energies of the leading configurations from the CASSCF calculations were done to predict the low-lying states. Ir_2 is a $^5\Delta$ and Ir_3 is linear with $^2\Delta$ state. We are currently preparing a manuscript on these structures. The structures and their energies are given in Figure 4. We will investigate the interactions of these clusters with zeolites and their cations in the acidic site of zeolite models. We will continue to investigate the reactions of the clusters following our work on the reactions of the Ir^+ ion in the acidic site of a zeolite where it has replaced a proton. Hydrogenation of small Ir clusters has also been investigated, with energy results summarized in Table 1.

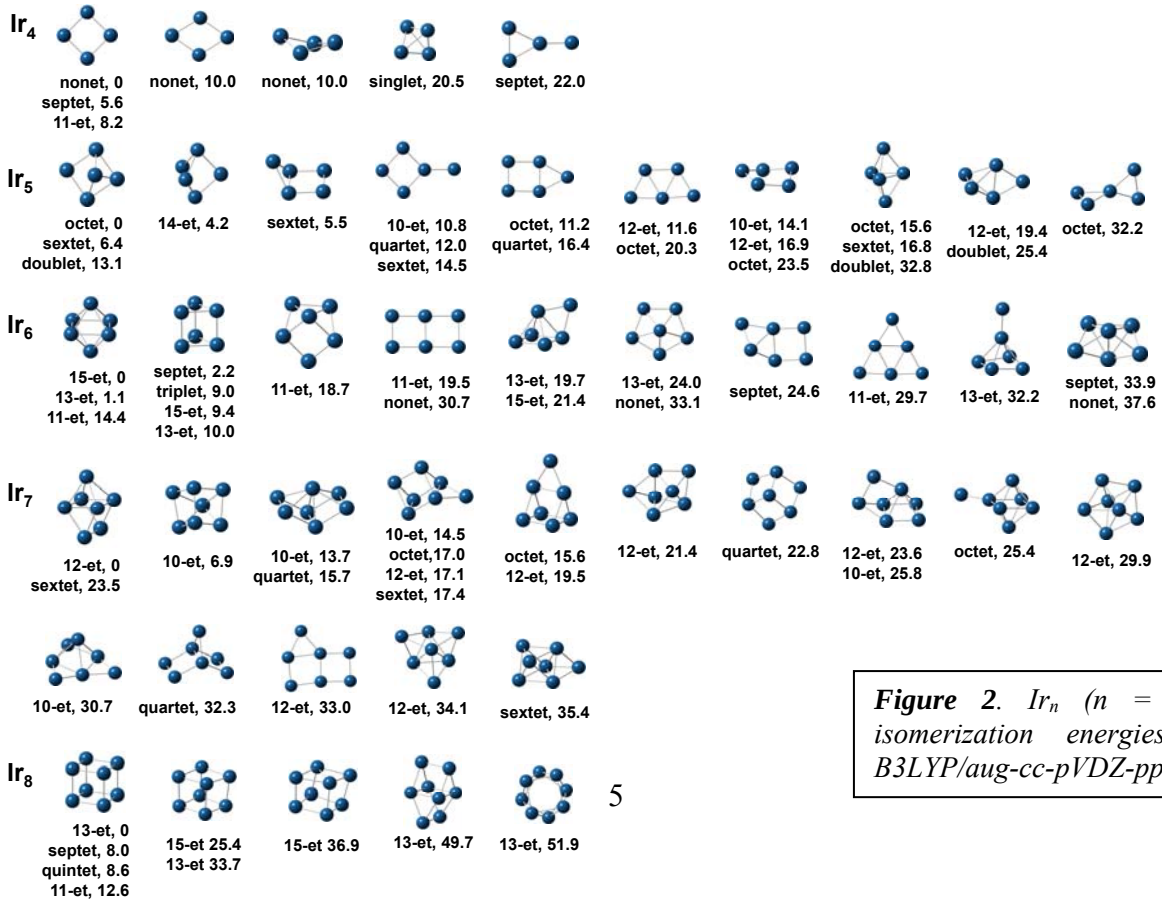

Figure 2. *Ir_n (n = 4-8) isomers and isomerization energies in kcal/mol at B3LYP/aug-cc-pVDZ-pp level.*

Table 1. *Reaction energies for the addition of H and H_2 to iridium clusters (in kcal/mol).*

Reaction (+H)	B3LYP/ad	R/UCCSD(T)/at	Reaction (+H_2)	B3LYP/ad	R/UCCSD(T)/at
Ir + H → IrH	-69.2	-74.8			
IrH + H → IrH_2	-71.0	-68.6	Ir + H_2 → IrH_2	-39.3	-41.1
IrH_2 + H → IrH_3	-81.3	-85.7	IrH + H_2 → IrH_3	-51.4	-52.0
IrH_3 + H → IrH_4	-40.6	-39.3	IrH_2 + H_2 → IrH_4	-21.0	-22.7
IrH_4 + H → IrH_5	-74.1	-77.8	IrH_3 + H_2 → IrH_5	-13.8	-14.9
IrH_5 + H → IrH_6	-42.3	-41.5	IrH_4 + H_2 → IrH_6	-15.5	-17.1
IrH_6 + H → IrH_7	-73.9	-78.1	IrH_5 + H_2 → IrH_7	-15.3	-17.3
IrH_7 + H → IrH_8	-38.0	-37.6	IrH_6 + H_2 → IrH_8	-11.0	-13.5
IrH_8 + H → IrH_9	-78.0	-81.5	IrH_7 + H_2 → IrH_9	-15.1	-16.9

The hydroxyl groups that terminate the surfaces of many oxides, including silica, are the principal grafting sites used to attach organic and organometallic compounds to the support. We have studied the structures of $GeCl_4$ grafted to a model of a hydrogenated silica surface leading to termination of OH bond. Geometries and frequencies were obtained at the MP2/aug-cc-pVDZ level with final energies at MP2/aug-cc-pVTZ. The results show that $GeCl^+$ can be grafted by two $Si(OH)_4$ groups as modes for two silica sites as shown in Figure 4. The reaction $GeCl_4(T_d)$ + $2Si(OH)_4$ → $GeCl_4$-$(Si(OH)_4)_2$ is exothermic as shown for the structures in Figure 4 as is the reaction $GeCl_4(T_d)$ + $2Si(OH)_3O^-$ → $GeCl_4$-$(Si(OH)_3O^-)_2$. These results are being used to analyze the experimental results of the S. Scott group at UCSB. A novel chemical finding is that the edge inversion barrier for GeCl4 of 57 kcal/mol is reduced to zero when the $(HO)Si(OH)_3$ group binds to the Ge.

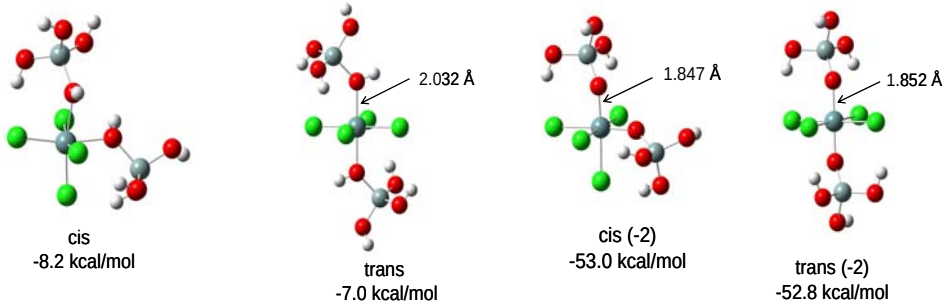

Figure 4. *Hexacoordinate Ge complexes with reaction energies for the reactions given in the text.*

Molecular Models of Site-Isolated Cobalt, Rhodium, and Iridium Catalysts Supported on Zeolites

Numerous zeolite- and oxide-supported metal complexes, an important class of catalysts, have been prepared from precursors incorporating metals with formal charges of +1 or +2 reacting with the acidic sites of the supports. Thoroughly investigated materials in this class include Group 9 metals on zeolite HY, Ir, Rh, and Ru complexes on zeolite Hβ, and Ir complexes on zeolite HSSZ-53. The Si/Al atomic ratios of the zeolites were chosen to be high (Si/Al = 30, 18, and 24, for zeolites Y, β, and SSZ-53, respectively) to allow formation of widely separated supported mononuclear species isolated at the Al sites. The nearly unique, well-defined structures of some of these site-isolated supported species were demonstrated by images of the isolated metal atoms obtained with high-resolution aberration-corrected scanning transmission electron microcopy. However, there were no data available on the bond energies of such species. The chemistry of zeolite-supported site-isolated cobalt, rhodium, and iridium complexes that are essentially molecular was investigated with density functional theory (DFT) and the results compared with experimentally determined spectra characterizing rhodium and iridium species formed by the reactions of $Rh(C_2H_4)_2(acac)$ and $Ir(C_2H_4)_2(acac)$ (acac = acetylacetonate) with acidic zeolites such as dealuminated HY zeolite. The experimental results characterize ligand exchange reactions and catalytic reactions of adsorbed ligands, including olefin hydrogenation and dimerization. Two molecular models (Figures 5 and 6) were used to characterize various binding sites of the metal complexes in the zeolites, and the agreement between experimental and calculated infrared frequencies and metal–ligand distances determined by extended X-ray absorption fine structure spectroscopy was generally very good. The calculated structures and energies indicate a metal–support-oxygen (M(I)–O) coordination number of two for most of the supported complexes and a value of three when the ligands include the radicals C_2H_5 or H. The results characterizing various isomers of the supported metal complexes incorporating hydrocarbon ligands indicate that some carbene and carbyne ligands could form. Ligand bond dissociation energies (LDEs) are reported to explain the observed reactivity trends. The experimental observations of a stronger M–CO bond than M–(C_2H_4) bond for both Ir and Rh match the calculated LDEs, which show that the single-ligand LDEs of the mono and dual-ligand complexes for CO are ~12 and ~15 kcal/mol higher in energy (when the metal is Rh) and ~17 and ~20 kcal/mol higher (when the metal is Ir) than the single-ligand LDEs of the mono and dual ligand complexes for C_2H_4, respectively. The results provide a foundation for the prediction of the catalytic properties of numerous supported metal complexes.

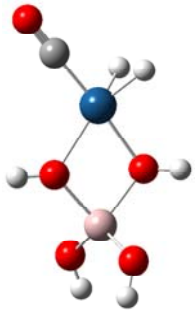

***Figure 5**. Ir(CO)(H_2) on the 2O sites of $Al(OH)_4^-$. Cyan: iridium. Red: oxygen. Gray: carbon. White: hydrogen.*

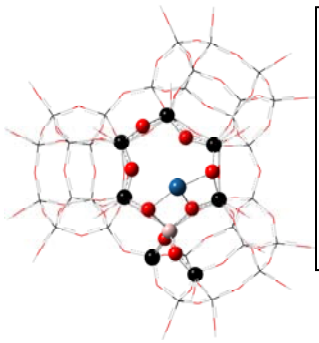

***Figure 6**. The Zeo(48-T)Ir model for the zeolite-supported Ir catalyst. The high layer is displayed in "ball and bond" mode, and the low layer as a wire frame.*

The simple M^+–$Al(OH)_4^-$ model provided geometries, vibrational frequencies, and LDEs characterizing the zeolite-supported Group 9 transition metal catalysts that are consistent with the limited amount of available experimental values for Rh and Ir and with the computational results based on the ONIOM calculations determined using the much larger Zeo(48-T)Ir model. The use of the $Al(OH)_4M$ model

greatly reduced the computational cost—yet still retained most of the key energetic features for the simulation of the Group 9 transition metal complex catalysts in a zeolite environment. Moreover, the use of the -D3 dispersion corrected functional did not substantially change the results for the Co complexes.

The ground-state structures of $Co(L_1)(L_2)Al(OH)_4$ complexes tend to be high-spin and have non-planar ligand coordination as a consequence of the tetrahedral ligand field, whereas most of the ground-state structures of $Rh(L_1)(L_2)Al(OH)_4$ and $Ir(L_1)(L_2)Al(OH)_4$ complexes are low-spin and have planar geometry in an octahedral ligand field. The differences between the geometry and stability of the Co complexes, and the Rh and Ir complexes, are related to the low-lying electronic states of the Co^+, Rh^+, and Ir^+ ions.

Binding of common ligands from the gas phase to the model structure $M–Al(OH)_4$ (M = Co, Rh, Ir) was investigated by using DFT, including calculations of the LDEs (Table 2), NBO charges, and vibrational frequencies. The calculated ligand dissociation energies show that the metal–ligand interaction strength has the following order: LDE(Ir–L) > LDE(Rh–L) > LDE(Co–L). The strength of the M–L bond is related to the electron density distribution in the ligand, which affects the reactivities in ligand activation reactions on the transition metal complex catalysts. Carbyne and carbene ligands, which are potential intermediates in the observed organic ligand activations, were found to be more stable on the Ir complexes than on the Rh or Co complexes. The results suggest that the Ir complex catalyst should be the best for C=C and H–H bond activation in terms of generating stable intermediates. The relative values of the calculated LDEs are consistent with the experimental results determined in transient IR and EXAFS experiments characterizing the Ir and Rh complexes with CO and C_2H_4. Good agreement was also found between the calculated and experimental ν_{CO} and ν_{CH} frequencies. The computational results provide the first reasonable estimates of these quantities for these types of single-site catalysts, and they can be used to improve catalyst design.

Table 2. *Calculated Average LDEs in kcal/mol for $M(L_1,L_2)$ and M(L) Complexes*

Ligand	$Ir(L_1,L_2)$[a]	$Rh(L_1,L_2)$	$Co(L_1,L_2)$[b]	Ir(L)[a]	Rh(L)	Co(L)[a]
H	70/77	59	44(44)	79/	56	72(72)
CO	69/70	50	28(33)	77/71	47	45(45)
C_2H_5	53[c]/59	42	17(20)	[c]/72	54[d]/44	56(58)
C_2H_2	50/54	36	12(16)	87/83	47	49(51)
C_2H_4	49/52	36	9(10)	60/47	35	39(43)
H_2	42/46	27	3(4)	54/45	22	26(27)
N_2	36/41	25	0(1)	45/43	23	19(19)

[a]*Values after the slash are for the LDEs calculated with the Zeo(48-T)Ir model.* [b]*-D3 results in parentheses.* [c]*M-L LDEs were calculated using the Zeo(48-T)Ir model for $Ir(C_2H_5)(L)$ as $Ir(C_2H_5)–Al(OH)_4$ is not a minimum energy structure.* [d]*agostic C_2H_5.*

The potential energy surfaces were calculated for the ethylene hydrogenation reaction catalyzed by the Ir, Rh, and Co complexes. The PES for the ethylene hydrogenation reaction on Ir has the deepest well depth among the three metals, implying that the Ir catalyst has the best performance in activation consistent with the experimental observation that Ir is more active than Rh. The zeolite supported Group 9 catalysts can have a CO bonded to the metal as the auxiliary ligand if $M(CO)_2(acac)$ was used as the precursor in the synthesis. For the hydrogenation reaction on the Ir catalysts, the auxiliary CO ligand can lower the stability of the various reaction intermediates, reduce the reaction barrier (which is correlated to the well depth) to release C_2H_6, and consequently improve the reaction efficiency. The ethylene hydrogenation PES largely depends on the electrophilicity of the isolated M site (with or without auxiliary ligands), which determines the M-C and M-H bond strengths. The reactivity of the hydrogenation reaction can be

improved by the choice of the metal, supports, and auxiliary ligands. Overall, the computational results together with the experimental observations provide a relatively complete picture of the catalytic hydrogenation of ethylene on single-site supported Rh and Ir catalysts and provide suggestions as to what to observe in future experimental investigations.

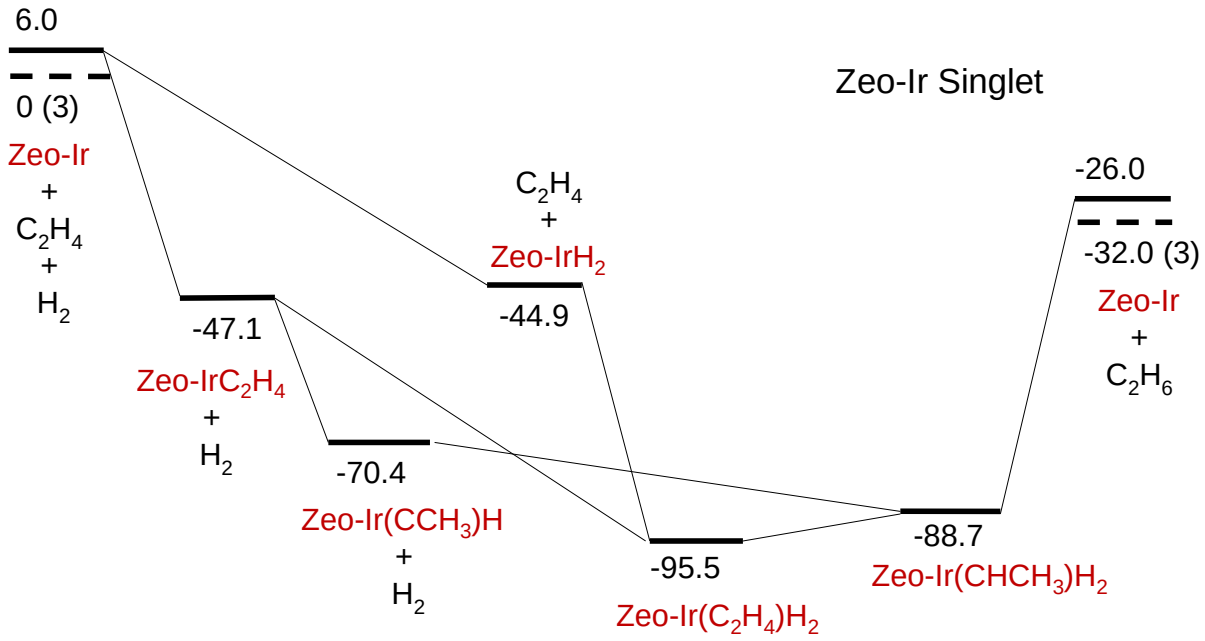

***Figure 7**. Potential energy surfaces with reaction energies (ΔE + ΔZPE) in kcal/mol characterizing the catalytic ethylene hydrogenation reaction on (a) Zeo(48-T)Ir at the ONIOM(B3LYP, PM6)/cc-pVDZ(-pp) level.*

Figures 7 and 8 show reactions of zeolite-supported Ir and Rh complexes with CO and C_2H_4 based on analyses of transient IR and EXAFS data. The experimental results show that all of the C_2H_4-containing complexes (i.e., $M(C_2H_4)(C_2H_4)$, $M(C_2H_4)(CO)$, and $M(C_2H_4)(C_2H_4)(CO)$) underwent fast and complete ligand exchange when brought in contact with a pulse of CO at 298 K and 1 bar, transforming each of the complexes into M(CO)(CO) without any detectable intermediates. In contrast, when M(CO)(CO) complexes were brought in contact with a continuous stream of C_2H_4, $M(CO)(CO)(C_2H_4)$ intermediate species were detected by IR spectroscopy. Moreover, treatments of M(CO)(CO) in C_2H_4 led to only partial ligand exchange, forming $M(C_2H_4)(CO)$ or $M(C_2H_4)(C_2H_4)(CO)$. These experimental observations suggest a stronger M–CO bond than M–(C_2H_4) bond for both Ir and Rh, precisely matching the calculated LDEs, which show that the single-ligand LDEs of the mono and dual-ligand complexes for CO are ~12 and ~15 kcal/mol higher in energy (when the metal is Rh) and ~17 and ~20 kcal/mol higher (when the metal is Ir) than the single-ligand LDEs of the mono and dual ligand complexes for C_2H_4, respectively. Furthermore, the calculated LDEs of C_2H_4 for Ir are significantly greater than for Rh (the differences are 25 and 15 kcal/mol for the single-ligand LDEs of the mono and dual ligand complexes, respectively), which explains the observation that when M(CO)(CO) is treated in C_2H_4, a mixture of $M(C_2H_4)(CO)$ and $M(C_2H_4)(C_2H_4)(CO)$ is formed when M = Ir, whereas when M = Rh, only $M(C_2H_4)(CO)$ is observed.

Computational investigation of Iridium Carbonyl Phosphine Clusters

Iridium clusters catalyze a wide range of reactions, including oxidation, hydrogenation, C–H bond activation, cycloaddition, cycloisomerization, and ring-opening. Iridium complexes play important roles in oxidation (e.g., of alcohols, phenols, and amines, hydrogenation, C-H activation, cycloaddition (e.g., [2 + 2 + 2], [2 + 2 + 1], and [4 + 2], cycloisomerization, and ring-opening reactions. Although there is significant interest in the catalytic properties of substituted iridium carbonyl clusters, there is little thermodynamic information available characterizing them.

Calculations of the structures and energetics of a range of $Ir_X(PH_3)_Y(CO)_Z$ (x = 1, 2, 4) have been performed. Benchmark calculations have been performed for the LDEs for the x = 1 and 2 clusters at the DFT level with 10 exchange-correlation functionals as well as at the correlated molecular orbital MP2 and CCSD(T) levels. The best agreement with CCSD(T) was found by using the ωB97X-D functional, and so it was used for the x = 4 LDE calculations. The doublet states of the $Ir(PH_3)_y(CO)_z$ clusters are significantly lower in energy than the quartet states. The carbonyls are stronger π-electron acceptor ligands than PH_3, and the PH_3 ligands act as stronger σ-electron donors and weaker π-electron acceptors than CO. Such electronic effects strengthen the Ir-C bond and increase the LDEs of the CO ligand for the complexes with a single Ir atom. The σ-electron donation ability of PH_3 provides more electron density on the Ir atom that can be used for π-back-bonding to the carbonyl. Yet this increased σ-electron donation leads to an increased repulsion with the d valence electrons from the Ir (often called Pauli repulsion). The balance of these two effects will govern the properties at the minimum for the mononuclear iridium complexes, and it is also relevant to the LDE if the properties of the Ir-containing product are similar. The trans influence of carbonyls is important in determining the structure, relative energies, and dissociation energies of these mononuclear iridium complexes. The isomers of these complexes with *ax* phosphines are of lower energy. The Ir–CO LDE increases with increasing substitution of CO by PH_3 ligands, whereas the LDEs of PH_3 ligands decrease slightly as more PH_3 ligands are added. IrL_4 complexes are more distorted, with lower LDEs, than IrL_3, and steric effects also play roles even in these small complexes.

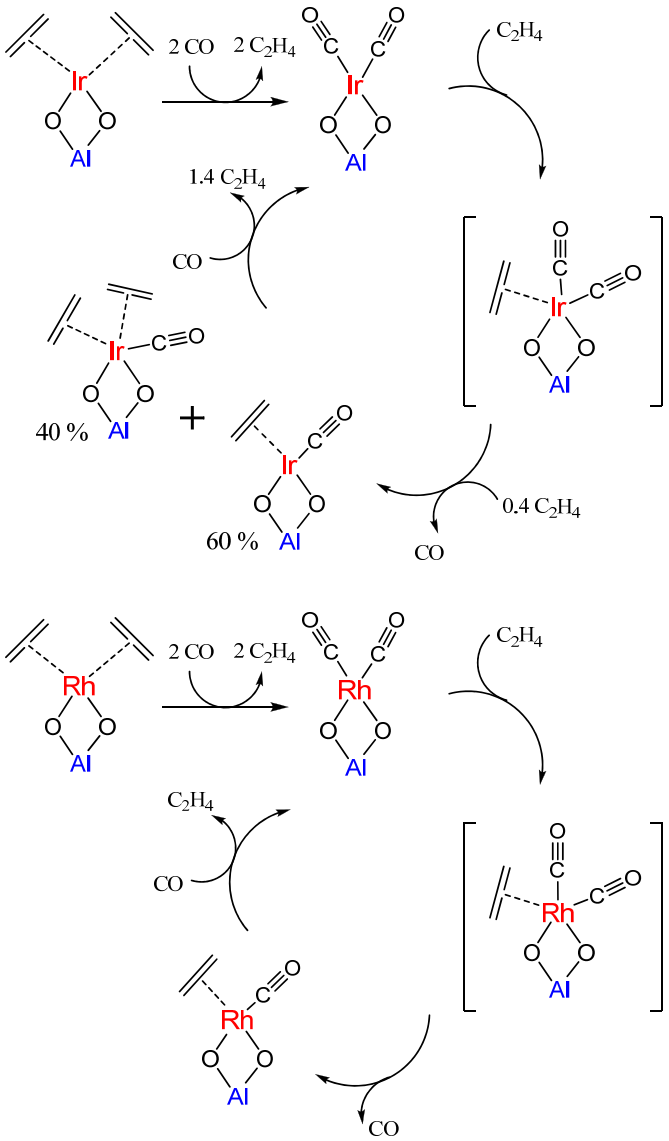

Figure 8. *Experimentally determined reactions of zeolite-supported Ir and Rh complexes with CO and C_2H_4 at 298 K and 1 bar.*

The three basic structures of $Ir_2(PH_3)_y(CO)_z$ isomers have C_{2v}, C_2, and D_{3d} symmetry. The two trans ligands along the Ir–Ir axis in the D_{3d} isomers are strongly bonded, leading to lower energy structures. The dissociation of such ligands results in higher energy isomers. C_2 and C_{2v} are coordinatively saturated isomers with energies that are close to each other, whereas the C_2 isomers of coordinatively unsaturated species are of lower energy. The changes are similar to those found for $Ir(PH_3)_y(CO)_z$ complexes as more PH_3 ligands are introduced. PH_3 substitution increases the negative charge on the Ir atom and strengthens the binding between the carbonyls and the Ir atom and slightly decreases the LDEs of the PH_3 ligands. This trend is the same as that predicted for $Ir(PH_3)_y(CO)_z$ complexes.

The C_{3v} structures of $Ir_4(PH_3)_y(CO)_z$ clusters have similar energies with respect to the T_d isomers for $Ir_4PH_3(CO)_{11}$ and $Ir_4(PH_3)_2(CO)_{10}$, and the C_{3v} structures are of even lower energy for $Ir_4(PH_3)_3(CO)_9$ and $Ir_4(PH_3)_4(CO)_8$. This conclusion is consistent with observations of C_{3v} structures for mono-phosphine Ir_4 clusters with larger and more electron-withdrawing R groups on the phosphorus. Our explanation for these energy differences is that the charge differences on the Ir atoms do not vary much from those in the $Ir_4(CO)_{12}$ T_d structure and that steric interactions are minimized. Structural transformations in the process of carbonyl dissociation can occur with T_d isomers converting into C_{3v} isomers; the reverse does not occur. Hydrogen atom transfer from a PH_3 usually occurs with a bridging carbonyl dissociation coupled with a weakly bonded PH_3 and results in a bridging phosphido group and an Ir–H bond that makes the cluster coordinatively saturated (Figure 9). A bridging PH_3 can move to an equatorial position as that *eq* carbonyl is dissociated. Such a transformation stabilizes the product cluster and reduces the LDEs. When hydrogen atom transfer and the rearrangement of the PH_3 from a *bri* to an *eq* position does not occur, the lowest CO LDE for a given site follows the order *eq* > *ax* > *bri* > *api*. Up to x = 3, the lowest-energy CO LDEs are approximately the same as PH_3 ligands are substituted for CO. Experimentally, an increase in the numbers of phosphines leads to an increase in the decarbonylation rates, most likely a consequence of the use of much bulkier phosphines and potentially kinetic control of the decarbonylation. The addition of the phosphines makes the Ir

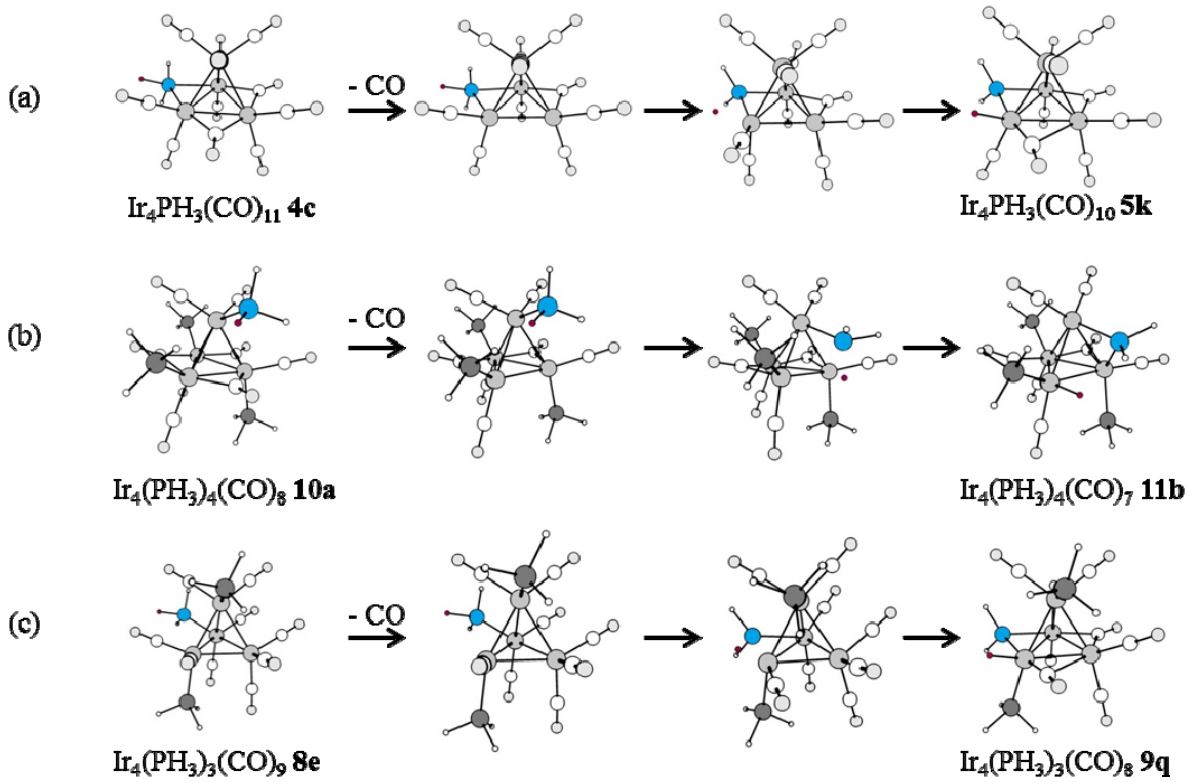

Figure 9. *Three types of H atom transfer reactions that occur on CO dissociation. The H and P atoms involved in the transfer reactions are marked in red and blue, respectively. The isomers in mid two columns are for description, not transition states or intermediates.*

atoms more electron rich, leading, it has been hypothesized, to a lower-energy transition state for thermal decarbonylation. The NBO calculations for the C_{3v} isomers show that the bridging carbonyls donate less electron density to the tetrairidium core (are less positive) than do the terminal carbonyls. The transition state for dissociation of a bridging carbonyl has more electron density on the tetrairidium core than those involving carbonyls in other sites, as shown by the charge distributions in the respective $Ir_4(CO)_{11}$ clusters. Thus, one should expect lower-energy transition states for the dissociation of bridging carbonyls. Because CO ligands can switch between the basal and bridging sites, basal substitution can occur more readily than apical substitution. Similar to the trend found for $Ir(PH_3)_y(CO)_z$ and $Ir_2(PH_3)_y(CO)_z$, the LDEs of the PH_3's in the tetra-iridium cluster gradually decrease with an increasing number of PH_3's.

Low-lying Electronic States of Ir_n Clusters with n = 2–8 Predicted at the DFT, CASSCF, and CCSD(T) Levels

Group VIII transition metal clusters play a prominent role in catalysis, for example, catalyzing organic reactions such as olefin hydrogenation, oligomerization, and ring opening of six-member ring cycloalkanes. The geometries of the low energy isomers for Ir_n, n = 2 to 8, were optimized using different DFT functionals and the CASSCF method. The $^5\Delta_g$ state is found to be the ground state for Ir_2, and the $^2\Delta_g$ state is found to be the ground state for Ir_3. We found that the spin orbit (SO) corrections are important in determining the ground spin state and the low energy excited states for Ir_2 and Ir_3. The total SO correction to the cluster molecules and the SO corrections per atom to the molecular SO correction decrease as the cluster size increases, and become small for n >3. The <AE> for Ir_n increases as n increases in general, and does not converge to the bulk limit by n = 8 (Table 3) . Including the SO correction in Ir_n <AE> will decrease the <AE> by ~15 kcal/mol for n ≥ 4. The ZPE and CV corrections to the <AE>'s are small as compared to the SO atomic correction, although the CV correction should be included if possible for the determination of the Ir_n ground states. We fit the calculated Ir_n <AE> versus n using logarithmic functions and used the experimental <AE> of 159.0 kcal/mol for bulk iridium at n = 1000. The <AE> vs n line for Ir_{2n+1} is slightly below the line for Ir_{2n}. At n = 200, the Ir_n cluster has an <AE> of ~120 kcal/mol, and the <AE> is predicted to be ~140 kcal/mol near n = 400.

Table 3. *Normalized Atomization Energies (<AE>, kcal/mol) for the Low Energy Isomers of Ir_n (n = 1 - 8) at CCSD(T) Level.*

Cluster	Spin	CBS + ΔE_{corr}	CBS + ΔE_{corr} +ΔE_{SO}[b]
Ir d^7s^2	4		
Ir d^8s^1	4	-6.5	
Ir_2 $D_{\infty h}$	5	40.8	31.1
Ir_2 $D_{\infty h}$	7	37.3	22.5
Ir_2 $D_{\infty h}$	3	34.7	21.1
Ir_3 $D_{\infty h}$	2	58.0	46.5
Ir_3 D_{3h}	4	56.1	41.4
Ir_4 D_{4h}	9	71.8	58.6
Ir_4 T_d	1	66.4	51.7
Ir_5 C_{4v}[c]	8	63.6	48.9
Ir_6 D_{4h}	13	86.1	71.4
Ir_6 O_h	15	85.6	71.0
Ir_7 C_{2v}	12	85.9	71.2
Ir_8 O_h	13	98.7	84.0
Expt			(159.0)

It is difficult to predetermine the best choice for a DFT exchange-correlation functional for specific problem without available benchmark data. As we have been using the B3LYP functional to study the chemistry of $Ir_x(CO)_y$ clusters, we chose it as the starting point for the DFT calculations in the current study. For the Ir_n clusters, we found that none of the three DFT functionals (B3LYP, PW91 and SVWN5) could predict the same ground state as did CCSD(T) calculations for all of the Ir_n (n = 2–8) clusters. The hybrid B3LYP predicted an incorrect ground state for Ir_3, and predicted the correct spin state but distorted geometry for Ir_5, mostly due to the symmetry breaking caused by the presence of Hartree-Fock exchange in the functional. For Ir_6, PW91 and SVWN5

predicted a septet structure to be the lowest energy isomer, whereas B3LYP and CCSD(T) agreed that the higher spin 13-et and 15-et octahedrons are the two lowest isomers. For Ir_8, B3LYP predicted the same cubic 13-et ground state as CCSD(T) predicted, whereas PW91 and SVWN5 predicted a quintet ground state which is ~40 kcal/mol higher in energy than the 13-et at the CCSD(T)/aD level. B3LYP clearly outperformed the PW91 and SVWN5 as n increased. This is a useful result as we are interested in the performance of DFT for larger clusters when the higher level CCSD(T) calculations cannot be performed as a consequence of the computational cost.

Structures and Stabilities of $Ir_n(CO)_m$

Iridium cluster carbonyl complexes ($Ir_n(CO)_m$) have been broadly investigated due to their interesting structures and their potential role in modeling catalytic processes. The most widely studied structure is $Ir_4(CO)_{12}$ and its derivatives have been used as homogeneous or supported catalysts for hydrocarbon activation as well as other processes. The clustering/carbonylation energies are summarized in Figure 6. The LDA SVWN5 functional predicts better geometries than the hybrid B3LYP functional for the $Ir_n(CO)_m$ clusters, but, as expected, LDA provides very poor energy results. Most of the bond length parameters by the SVWN5 are within 0.01 Å of the available experimental crystallography data. The optimized ground states of the $Ir_n(CO)_m$ clusters are low-spin (i.e., singlet or doublet). Relative energies of the isomers for each $Ir_n(CO)_m$ are calculated at the CCSD(T)//SVWN5 and DFT levels, the latter with a range of functionals. The average values of the CAM-B3LYP and B97-D relative energies ($\Delta E_{ave\text{-}DFT}$(Rel)) can be used to predict the relative energies of the various isomers of a given cluster when the higher level CCSD(T) cannot be performed. Using $\Delta E_{ave\text{-}DFT}$(Rel), the T_d structure of the $Ir_6(CO)_{16}$ is predicted to be ~2 kcal/mol more stable than the D_{2d} structure. CAM-B3LYP is the best functional to use for the prediction of the CO ligand dissociation energies for $Ir_n(CO)_m$, whereas ωB97X-D had the best performance in calculating the total dissociation energies of $Ir_n(CO)_m$ complexes. However, none of the DFT functionals can predict high quality reaction energies for the nucleation reactions of the $Ir_n(CO)_m$ clusters. An estimate of the nucleation reaction energies can be made by taking the average of the ωB97X-D and MP2 energies which gives semi-quantitative results in comparison to the CCSD(T) values. The DFT methods predict reaction energies that are less negative than the CCSD(T) values whereas the MP2 method predicts reactions energies that are more negative. These average values can be used to calculate the reaction energies for the nucleation reactions where it was too computationally expensive to calculate the CCSD(T) values. In addition, pure GGA functionals failed to predict both the relative energies and the reaction energies for $Ir_n(CO)_m$. They are not a reliable method for the class of molecules studied in this work. The self-assembly reactions from the mono-nuclear clusters to form larger clusters are all exothermic. $Ir_4(CO)_{12}$ is calculated to be the most energetically favored $Ir_n(CO)_m$ cluster at 0 K, and its conversion to $Ir_6(CO)_{16}$ requires higher temperatures and pressures.

See Figure 10 for a reaction energy diagram for the nucleation reaction of $Ir_n(CO)_m$ at 0 K.

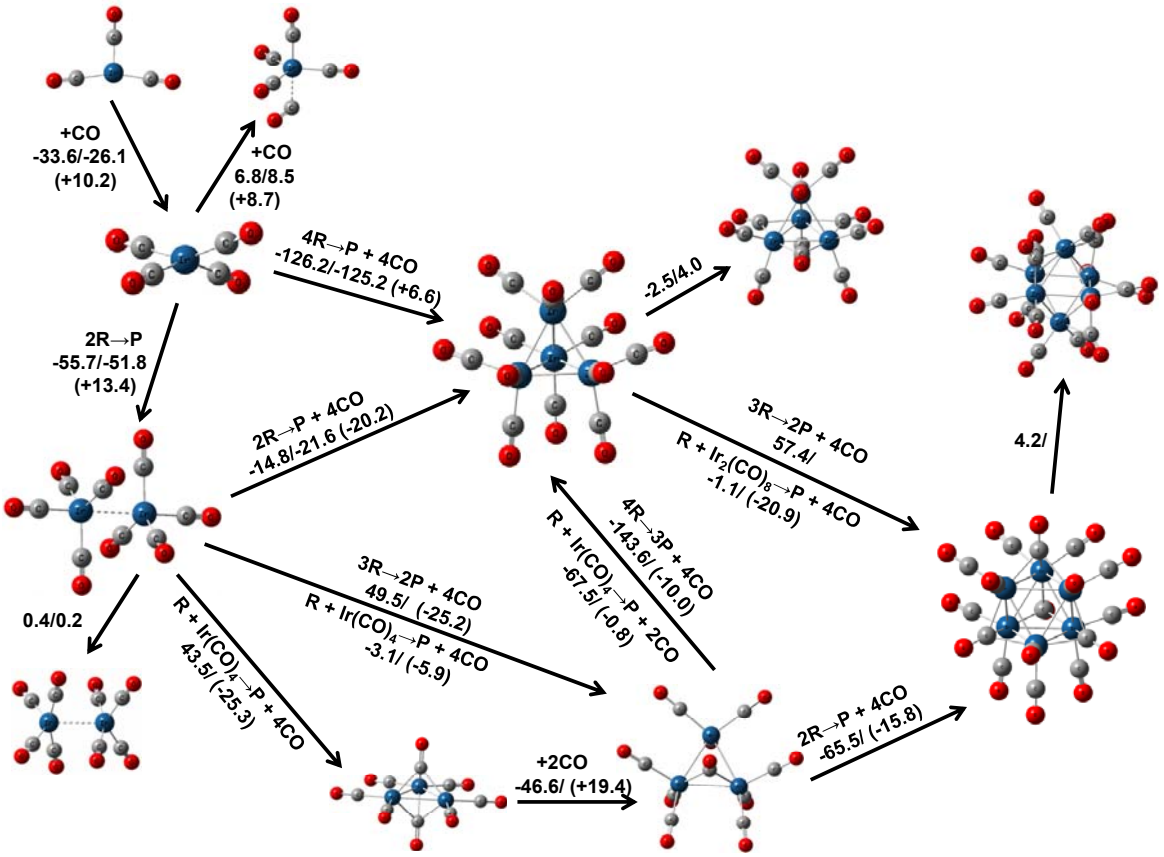

Figure 10. *Reaction energy diagram for the nucleation reaction of $Ir_n(CO)_m$ at 0 K. Energies are in kcal/mol. The values before the "/" are the average value of the MP2 and ωB97X-D reaction enthalpy at 0 K. The values after the "/" are the CCSD(T) reaction enthalpy at 0 K, and left blank if no CCSD(T) energy is available. Values in parenthesis are Gibbs free energy correction to the reaction energy at 298 K.*

Synthesis, characterization, reactivities, and catalytic properties of zeolite supports and supported iridium clusters

The first stage of the research project from the characterization side is to understand the morphology of the zeolite support both in 2 dimensions (2-D) on the atomic scale, and in 3 dimensions (3-D) on the nanoscale. Delaminated zeolites have been found to provide a higher surface area by about a factor of 2–3, and we aim to synthesize and characterize our delaminated materials on the nanoscale. The precursor material is MCM-22(P), and the delaminated materials are UCB-1 and ITQ-2. UCB-1 has been shown to have superior properties to ITQ-2 due to a lack of an amorphous phase in the materials.

The electron microscopy was performed on an aberration corrected (image corrected) FEI Environmental Titan instrument at the Environmental Molecular Sciences Laboratory (EMSL) at PNNL. Analysis was performed at both 80 kV and 300 kV to understand the effects of beam damage and charging on these particular zeolites and to image them accordingly. Electron tomography was performed in STEM mode

after a thin (~5 nm) coating of carbon was sputtered onto the TEM grid in order to reduce or eliminate zeolite motion due to charging by the electron beam.

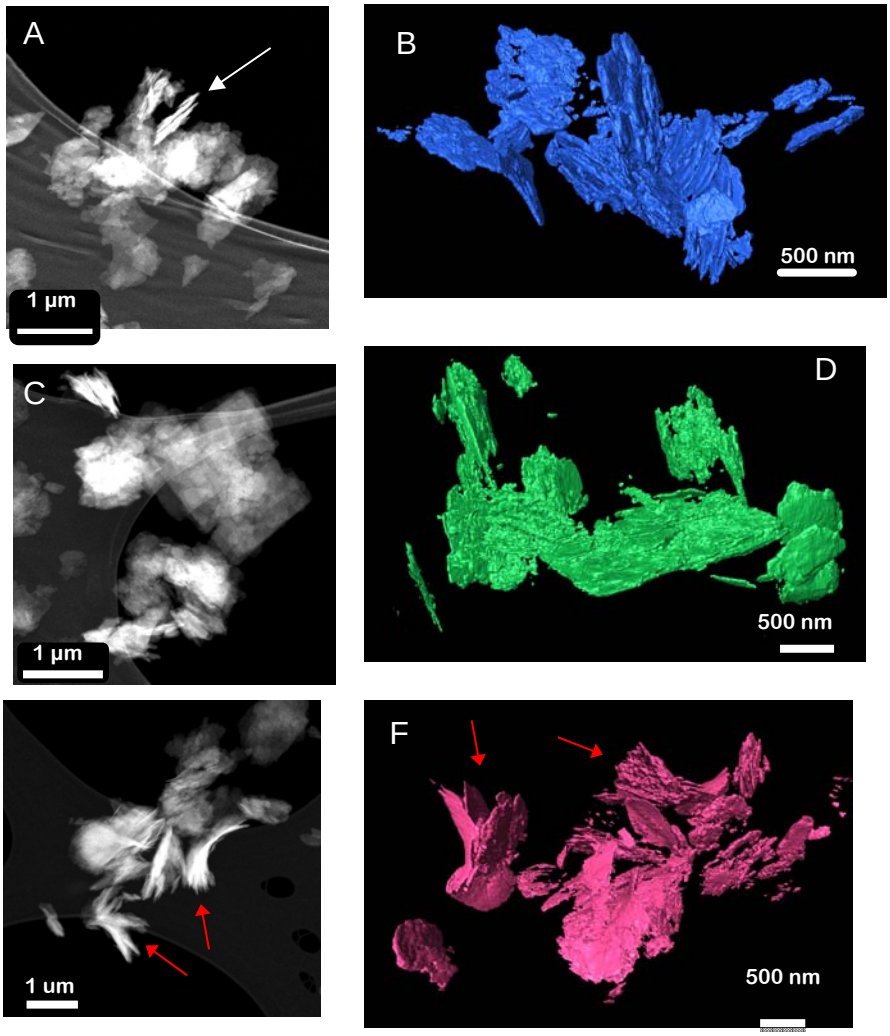

Figure 11. *Tomographic images demonstrating the progress of delamination of a zeolite (in sequence from A-F). The arrows show delaminated sheets. (A-C) show images from a tilt series at approximately -70°, 0°, and +70° of tilt in the microscope for UCB-1. The arrows highlight regions that show curved layers in this delaminated material. (D) shows a 1 nm slice through a reconstruction of the data, showing the spacing and distribution of the layers more clearly.*

Electron (STEM) tomography was performed on three sets of materials to determine the morphology of the materials and gain insight into the delamination process. The starting material was MCM-22 (P), which has been reported (as we confirmed) to consist of stacks of many flat layers. Figure 11A shows a 2-D STEM image, with an arrow indicating a stack of the flat layers, and Figure 11B shows the 3-D reconstruction of this material, providing a 3-D visualization of the stacks of flat layers. Upon treatment of the MCM-22 with an aqueous solution containing cetyltrimethylammonium bromide, tetrabutylammonium fluoride, and tetrabutylammonium chloride at a pH of 9 and 353 K, a new material formed, which we call UCB-1 uncalcined. The 2-D and 3-D characteristics of this material are similar to those of MCM-22 in that the layers of zeolite are still flat and closely packed. However, it is known (or

has at least been assumed) that the chemical treatment serves to break many of the bonds between the zeolitic sheets, because when UCB-1 is calcined at 823 K, a very different morphology emerges. The 2-D and 3-D morphologies of UCB-1 calcined are different from the morphologies of the precursor materials in two ways: first, the layers are curved and peeled open, exposing much more surface area than the precursor materials. Second, the distance between clusters is also greater, which again provides evidence of higher surface area and greater spaces for bulky molecules to enter and react.

This type of direct visualization of the delamination process is unprecedented and provides much important information on the synthesis process to guide future delamination syntheses.

A New Discrete Tomographic Reconstruction Method for Electron Tomography

We developed a new and advanced reconstruction algorithm for electron tomography data using a combination of compressed sensing and discrete reconstruction methods. Our algorithm not only provides accurate reconstructions with limited projection images, but also with a limited tilt range. This algorithm offers a solution to the decades-old "missing wedge" artifact present in reconstructions with limited data. With the ability to provide high quality reconstructions with only ~30 images as opposed to the standard ~120, this algorithm opens the door to materials characterization of electron beam sensitive materials across all fields of science. This 3-D characterization method with 1nm to sub-nm resolution provides a new methodology for the advancement of nanotechnology.

The reduced number of images necessary for a robust 3-D reconstruction also opens the door for 3-D chemical imaging, using EDX or EELS, where the number of tilts at which data are acquired is also limited. Standard methods of 3D reconstruction, such as weighted back projection (WBP) and simultaneous iterative reconstruction technique (SIRT), are not equipped to handle this lack of information, and result in significant blurring. Two of the recent successful algorithms are the discrete algebraic reconstruction technique (DART) and total variation (TV) minimization within compressed sensing (CS). The DART algorithm uses an algebraic reconstruction method (ARM) and pairs it with the prior knowledge that there are only a small number (two or three) of different materials in the sample, each corresponding to a different gray value in the reconstruction. An initial reconstruction is computed using the ARM and rounded to the chosen fixed gray values based on some threshold, and iteratively refined using the ARM. The method of TV minimization stems from the mathematical theory of compressed sensing and only recently became available due to new computational methods for solving the TV minimization problem. The method considers the characterization of real images and encourages the reconstruction to take larger jumps in gray values to create clear boundaries, hence creating a similar effect to that of DART. Examples of these methods will be presented, covering different material geometries, such as layered zeolite materials, porous supports, and particles in supports.

Experimental Evidence of First steps of metal cluster formation

The formation of iridium clusters from supported mononuclear iridium complexes in H_2 at 300 K and 1 bar was investigated by spectroscopy and atomic-resolution scanning transmission electron microscopy. The first steps of cluster formation from zeolite-supported $Ir(C_2H_4)_2$ complexes are triggered by the activation of H_2 and the formation of iridium hydride, accompanied by the breaking of iridium–support bonds. This reactivity can be controlled by the choice of ligands on the iridium, which include the support.

By use of the precursor $Ir(CO)_2(acac)$, a ship-in-a-bottle synthesis was used to prepare $Ir_6(CO)_{16}$ and, by decarbonylation, clusters well approximated as Ir_6 in the supercages of zeolite NaY. The samples were characterized by infrared and extended X-ray absorption fine structure (EXAFS) spectroscopies and imaged by aberration-corrected scanning transmission electron microscopy with a high dose electron

beam (~10^8 $e^-/Å^2$, 200 kV), and the catalyst performance was characterized by turnover frequencies for ethylene hydrogenation at 298 K and atmospheric pressure. The images characterizing a sample with about 17% of the supercages occupied by decarbonylated nanoclusters indicated clusters well approximated as Ir_6, with diameters consistent with such clusters, and some of the images show the clusters with atomic resolution and indicating each of the 6 Ir atoms. The cluster size was confirmed by EXAFS spectra. Two bonding positions of the Ir_6 clusters in the supercages were distinguished; 25% of the clusters were present at T5 sites and 75% at T6 sites. The results represent the first example of the application of high-dose electron beam conditions to image metal nanoclusters in a nanoporous material; the data are characterized by a high signal-to-noise ratio, and their interpretation does not require any image processing or simulations. These statements are based on images determined in the first 5 s of exposure of the catalyst to the electron beam; thereafter, the electron beam caused measurable deterioration of the zeolite framework and thereupon aggregation of the iridium clusters.

Using aberration-corrected STEM, we imaged iridium atoms in isolated iridium complexes in the one-dimensional nonintersecting 14-ring channels of zeolite SSZ-53. STEM allows tracking of the movement of atoms in the channels, demonstrating the interaction of iridium with the zeolite framework (channel confinement) and providing a direct visualization of the initial steps of metal nanocluster formation. The results demonstrate how STEM can be used to help design improved catalysts by identifying the catalytic sites and observing how they change in reactive atmospheres.

A major challenge in the use of supported metal nanocluster catalysts is to prevent deactivation by sintering of the clusters during operation. When sintering-driven deactivation has occurred, the catalysts typically require expensive and time-consuming regeneration processes to re-disperse the metals and recover their properties. There is therefore a strong incentive to discover and apply catalysts that are intrinsically resistant to sintering. Here we report atomic-scale observations of iridium nanoclusters supported on MgO demonstrating that the nanoclusters aggregate to reach a critical diameter of ~1 nm and then resist further aggregation from coalescence. These observations are consistent with theoretical predictions of the stability of iridium nanoclusters attaining a critical size and highlight the potential for this "smart" catalyst system to naturally assemble into stable clusters that are catalytically active. We recorded a movie demonstrating the nanoclusters of the critical size bounce off each other without aggregating.

Supported Bimetallic Catalysts with Segregated Metals

A family of supported bimetallic samples was prepared by the reactions of $Rh(C_2H_4)(acac)$ (acac = acetylacetonate) and $Os_3(CO)_{12}$ with MgO. The samples were characterized by IR and EXAFS spectroscopies, before and after various treatments with hydrogen at temperatures up to 393 K. The spectra identify the following combinations of supported species: (a) $[Os_3(CO)_{11}]^{2-}$ + $Rh(C_2H_4)_2$, (b) $[Os_3(CO)_{11}]^{2-}$ + $Rh(CO)_2$, and (c) $[Os_3(CO)_{11}]^{2-}$ + rhodium clusters containing approximately 4 to 6 atoms each, on average. No bimetallic clusters formed. The triosmium frame remained intact while the rhodium surface species were reduced in the presence of H_2. The samples were tested as catalysts for ethylene hydrogenation at 298 K, and the catalytic activity matched that of the rhodium complexes alone; evidently the rhodium complexes were responsible for all the catalysis, with the osmium clusters remaining inactive because of the presence of the carbonyl ligands on them.

Controlling the Formation of Supported Metal Clusters from Mononuclear Metal Complexes

Extremely small supported rhodium clusters were prepared from rhodium complexes on the surfaces of solids with contrasting electron-donor properties. The samples were characterized by infrared and extended X-ray absorption fine structure spectroscopies to characterize the changes occurring in the

rhodium species resulting from treatments in hydrogen. Rhodium cluster formation occurred in the presence of H_2, and the first steps are controlled by the electron-donor properties of the support—which acts as a ligand—and the other ligands bonded to the rhodium. The cluster formation begins at a lower temperature when the support is zeolite HY than when it is the better electron-donor MgO, provided that the other ligands on rhodium are ethylene. In contrast, when these other ligands are CO, the pattern is reversed. The choice of ligands including the support also allows regulation of the stoichiometry of the surface transformations and the stability of the structures formed in the presence of H_2. The combination of MgO as the support and ethylene as a ligand allows restriction of the cluster size to the smallest possible—which could be formed in high yields. The data are among the first characterizing the first steps of metal cluster formation.

Selective Molecular Recognition by Nanoscale Environments in a Supported Iridium Cluster Catalyst

Control of accessibility to a tetrairidium cluster surface is facilitated by synthetic nanopockets associated with three calixarene phosphine ligands. Vacancies are created on the cluster by removal of initially present CO ligands by either simple dissociation in flowing gas or, alternatively, by a new method consisting of reactive decarbonylation with the bulky reactant trimethylamine-N-oxide. Both methods lead to the synthesis of nanopockets that are accessible to CO, but only reactive decarbonylation creates such nanopockets that are also accessible to ethylene—and sites that catalyze its hydrogenation. The concept of synthesizing vacancies on the surface of a metal and simultaneously creating nanopockets that can act as selective molecular gatekeepers for controlling access to them may have wide-ranging applications in areas such as nanosensing, catalysis, and gas separations.

Published Review: Supported Molecular Metal Catalysts

Recent advances in the synthesis and characterization of small, essentially molecular metal complexes and metal clusters on support surfaces have brought new insights to catalysis and point the way to systematic catalyst design. We summarize recent work unraveling effects of key design variables of site-isolated catalysts: the metal, metal nuclearity, support, and other ligands on the metals, also considering catalysts with separate, complementary functions on supports. The catalysts were synthesized with the goal of structural simplicity and uniformity to facilitate incisive characterization. Thus, they are essentially molecular species bonded to porous supports chosen for their high degree of uniformity; the supports are crystalline aluminosilicates (zeolites) and MgO. The catalytic species are synthesized in reactions of organometallic precursors with the support surfaces; the precursors include $M(L)_2$(acetylacetonate)$_{1-2}$, with M = Ru, Rh, Ir, or Au and the ligands L = C_2H_4, CO, or CH_3. $Os_3(CO)_{12}$ and $Ir_4(CO)_{12}$ are used as precursors of supported metal clusters, and some such catalysts are made by ship-in-a-bottle syntheses to trap the clusters in zeolite cages. The simplicity and uniformity of the supported catalysts facilitate precise structure determinations, even in reactive atmospheres and during catalysis. The methods of characterizing catalysts in reactive atmospheres include IR, EXAFS, XANES, and NMR spectroscopies, and complementary methods include density functional theory and atomic-resolution aberration-corrected scanning transmission electron microscopy for imaging of individual metal atoms. IR, NMR, XANES, and microscopy data demonstrate the high degrees of uniformity of well-prepared supported species. The characterizations determine the compositions of surface metal complexes and clusters, including the ligands and the metal-support bonding and structure, which identify the supports as ligands with electron-donor properties that influence reactivity and catalysis. Each of the catalyst design variables has been varied independently, illustrated by mononuclear and tetranuclear iridium on zeolite HY and on MgO and by isostructural rhodium and iridium (diethylene or dicarbonyl) complexes on these supports. The data provide examples resolving the roles of the catalyst design variables and place the catalysis science on a firm foundation of organometallic chemistry linked with

surface science. Supported molecular catalysts offer the advantages of characterization in the absence of solvents and with surface-science methods that do not require ultrahigh vacuum. Families of supported metal complexes have been made by replacement of ligands with others from the gas phase. Spectroscopically identified catalytic reaction intermediates help to elucidate catalyst performance and guide design. The methods are illustrated for supported complexes and clusters of rhodium, iridium, osmium, and gold used to catalyze reactions of small molecules that facilitate identification of the ligands present during catalysis: alkene dimerization and hydrogenation, H-D exchange in the reaction of H_2 with D_2, and CO oxidation. The approach is illustrated with the discovery of a highly active and selective MgO-supported rhodium carbonyl dimer catalyst for hydrogenation of 1,3-butadiene to give butenes.

Summary of interactions among PI's, their groups, and other collaborators

The zeolites and the unsupported metal cluster samples were synthesized in Berkeley and the supported samples in Davis and Berkeley, with the calculations done in Alabama and the TEM done at PNNL and in Davis. The spectroscopy experiments were done in Berkeley and Davis and at SSRL and BNL. Catalysis experiments were done in Davis and Berkeley. The collaborators conferred frequently regarding sample synthesis and modification, experiments, calculations, and physical characterizations. For example, the delaminated zeolites prepared in Berkeley were investigated extensively in tomography/TEM experiments at PNNL, and supported tetrairidium cluster samples prepared in Berkeley were investigated by STEM and IR spectroscopy in reactive atmospheres at Davis. Other samples were transferred to PNNL for tomography/TEM. The collaborators conferred by phone and email and at meetings such as the Annapolis DOE PI meetings and ACS and AIChE meetings.

Publications

"Ir_6 Clusters Compartmentalized in the Supercages of Zeolite NaY: Direct Imaging of a Catalyst with Aberration-Corrected Scanning Transmission Electron Microscopy," C. Aydin, J. Lu, M. Shirai, N. D. Browning, and B. C. Gates, *ACS Catal.*, **1**, 1613 (2011). Also supported by DOE BES grant DE-FG02-03ER46057, to Browning.

"Tracking Iridium Atoms with Electron Microscopy: First Steps of Metal Nanocluster Formation in One-Dimensional Zeolite Channels," C. Aydin, J. Lu, A. J. Liang, C.-Y. Chen, N. D. Browning, and B. C. Gates, *Nano Lett.*, **11**, 5537 (2011). Also supported by BES grant DE-FG02-03ER46057, Browning. Time of Chevron researchers Liang and Chen supported by Chevron.

"Matrix Infrared Spectroscopic and Electronic Structure Investigations of the Lanthanide Metal Atom-Methyl Fluoride Reaction Products CH_3-LnF and CH_2-LnHF. The Formation of Single Carbon-Lanthanide Metal Bonds," M. Chen, D. A. Dixon, X. Wang, H.-G. Cho, and L. Andrews *J. Phys. Chem. A*, **2011**, *115*, 5609–5624.

"Infrared Spectra and Quantum Chemical Calculations of the Bridge Bonded HC(F)LnF_2 (Ln = La-Lu) Complexes," Y. Gong, X. Wang, L. Andrews, M. Chen, and D. A. Dixon, *Organometallics*, **2011**, *30*, 4443–4452.

"Hydrogen Activation and Metal Hydride Formation Trigger Cluster Formation from Supported Iridium Complexes," J. Lu, C. Aydin, N. D. Browning, and B. C. Gates, *J. Am. Chem. Soc.*, **134**, 5022 (2012). Also supported by DOE BES grant DE-FG02-03ER46057 to Browning.

"A Smart Catalyst: Sinter-resistant Supported Iridium Clusters Visualized with Electron Microscopy," C. Aydin, J. Lu, N. D. Browning, B. C. Gates, *Angew. Chem. Int. Ed.,* 51, 5929 (2012). Also supported by DOE BES grant DE-FG02-03ER46057 to Browning.

"Gold nanoparticle-catalyzed reduction in a model system: Quantitative determination of reactive heterogeneity of a supported nanoparticle surface," M. Nigra, I. Arslan, A. Katz, *J. Catal.*, **295**, 115 (**2012**).

"Structures and Stability of $Ir_n(CO)_m$," M. Y. Chen, J. E. Dyer, B. C. Gates, A. Katz, and D. A. Dixon, *Mol. Phys.*, **110**, 1977 (2012).

"Sinter-Resistant Catalysts: Supported Iridium Nanoclusters with Intrinsically Limited Sizes," J. Lu, C. Aydin, N. D. Browning, L. Wang, and B. C. Gates, *Catal. Lett.,* **142**, 1445 (2012). Also supported by DOE BES grant DE-FG02-03ER46057 to Browning.

"Three-Dimensional Structural Analysis of MgO-Supported Osmium Clusters by Electron Microscopy with Single-Atom Sensitivity," C. Aydin, A. Kulkarni, M. Chi, N. D. Browning, and B. C. Gates, *Angew. Chem. Int. Ed.*, **4**, 5262 (2013). Also supported by DOE BES grant DE-FG02-03ER46057 to Browning.

"MgO-Supported Bimetallic Catalysts Consisting of Segregated, Essentially Molecular Rhodium and Osmium Species," J. D. Kistler, P. Serna, and B. C. Gates, *Dalton Trans.,* **42**, 12626 (2013). Also supported by European Union grant to Serna.

"Quantitative *Z*-Contrast Imaging of Supported Metal Complexes and Clusters–A Gateway to Understanding Catalysis on the Atomic Scale," N. D. Browning, C. Aydin, J. Lu, A. Kulkarni, N. L. Okamoto, V. Ortalan, B. W. Reed, A. Uzun, and B. C. Gates, *ChemCatChem*, **5**, 2673 (2013). Also supported by DOE BES grant DE-FG02-03ER46057 to Browning and by DOE BES grant DE-FG02-04ER15513 to Gates.

"Supported gold catalysts: new properties offered by nanometer and sub-nanometer structures," B. C. Gates, *Chem. Commun.* **49**, 7876 (2013).

"Computational Study of the Low-lying Electronic States of Ir_n Clusters with n = 2 – 8 at the DFT, CASSCF, and CCSD(T) Levels," M. Chen and D. A. Dixon *J. Phys. Chem. A,* **2013**, *117*, 3676.

"Formation of supported rhodium clusters from mononuclear rhodium complexes controlled by the support and ligands on rhodium," P. Serna, D. Yardimci, J. D. Kistler, and B. C. Gates, *Phys. Chem. Chem. Phys.*, **16**, 1262 (2014). Also supported by DOE BES grant DE-FG02-04ER15513 to Gates.

"Selective molecular recognition by nanoscale environments in a supported iridium cluster catalyst," A. Okrut, R. C. Runnebaum, X. Ouyang, J. Lu, C. Aydin, S.-J. Hwang, S. Zhang, O. A. Olantunji-Ojo, K. A. Durkin, D. A. Dixon, B. C. Gates, and A. Katz, *Nat. Nanotechnol.*, **9**, 459 (2014). Also supported by DOE BES grant DE-FG02-03ER46057 to Browning and by NSF grant no. 9724240 for the NMR facility at Caltech.

"A Single-Site Platinum CO Oxidation Catalyst in Zeolite KLTL: Microscopoic and Spectroscopic Determination of the Locations of the Platinum Atoms," J. D. Kistler, N. Chotigkrai, P. Xu, B. Enderle, P. Praserthdam, C.-Y. Chen, N. D. Browning, and B. C. Gates, *Angew. Chem. Int. Ed.*, **53**, 8904 (2014). Also supported by DOE BES grant DE-FG02-04ER15513 to Gates.

"Molecular Metal Catalysts on Supports: Organometallic Chemistry Meets Surface Science," P. Serna and B. C. Gates, *Acc. Chem. Res.*, **47**, 2612 (2014). Also supported by DOE BES grant DE-FG02-04ER15513 to Gates.

"Identification of Binding and Reactive Sites in Metal Cluster Catalysts: Homogeneous–Heterogeneous Bridges," A. Katz, M. M. Nigra, in *Bridging Heterogeneous and Homogeneous Catalysis: Concepts, Strategies, and Applications*, C. Li, Y. Liu, Eds.; Wiley-VCH: Weinheim, Germany, 2014, Chapter 9.

"Beyond Relationships between Homogeneous and Heterogeneous Catalysis," D. A. Dixon, A. Katz, I. Arslan, and B. C. Gates, *Catal. Lett.*, **144**, 1785 (2014).

"Mononuclear iridium dinitrogen complexes bonded to zeolite HY," D. Yang, M. Chen, C. Martinez-Macias, D. A. Dixon, and B. C. Gates, *Chem. Eur. J.,* **21**, 631 (2015). Also supported by DOE BES grant DE-FG02-04ER15513 to Gates.

"Agglomerative Sintering of an Atomically Dispersed Ir_1/Zeolite Y Catalyst: Compelling Evidence Against Ostwald Ripening but for Bimolecular and Autocatalytic Agglomeration Catalyst Sintering Steps," E. Bayram, J. Lu, C. Aydin, N. D. Browning, S. Ozkar, E. Finney, B. C. Gates, and R. Finke, *ACS Catal.,* **5**, 3514 (2015). Also supported by DOE BES grant DE-FG02-03ER46057 to Browning and by DOE BES grant DE-FG02-03ER15433 to Finke.

"Imaging Individual Lanthanum Atoms in Zeolite Y by Scanning Transmission Electron Microscopy: Evidence of Lanthanum Pair Sites," P. Xu, J. Lu, C. Aydin, L. Debefve, N. D. Browning, C.-Y. Chen, and B. C. Gates, *Micropor. Mesopor. Matl.*, **213**, 95 (2015). Also supported by DOE BES grant DE-FG02-04ER15513 to Gates.

"Genesis of Delaminated-Zeolite Morphology: 3-D Characterization of Changes by STEM Tomography," I. Arslan, J. D. Roehling, I. Ogino, K. J. Batenburg, S. I. Zones, B. C. Gates, and A. Katz, *J. Phys. Chem. Lett.*, **6**, 2598 (2015). Also supported by PNNL LDRD program.

"Structures, Relative Energies, and Ligand Dissociation Energies of Iridium Carbonyl Phosphine Clusters," S. Zhang, A. Katz, B. C. Gates, and D. A. Dixon, *Comp. Theor. Chem.*, **1069**, 18 (2015).

"Single-Site Zeolite-Anchored Organoiridium Carbonyl Complexes: Characterization of Structure and Reactivity by Spectroscopy and Computational Chemistry," C. Martinez Macias, M. Chen, D. A. Dixon, and B. C. Gates, *Chem. Eur. J.*, **21**, 11825 (2015). Also supported by DOE BES grant DE-FG02-04ER15513 to Gates.

"Cooperative Catalysis on Solid Surfaces versus Soluble Molecules," A. Katz, N. M. Nigra, in *Cooperative Catalysis: Designing Efficient Catalysts for Synthesis,* R. Peters, Ed.; Wiley-VCH: Weinheim, Germany, 2015, Chapter 12.

"Molecular Models of Site-Isolated Cobalt, Rhodium, and Iridium Catalysts Supported on Zeolites: Ligand Bond Dissociation Energies," M. Chen, P. Serna, J. Lu, B. C. Gates, and D. A. Dixon, *Comp. Theor. Chem.*, in press (2015).